NJC

Accepted Manuscript

This is an *Accepted Manuscript*, which has been through the Royal Society of Chemistry peer review process and has been accepted for publication.

Accepted Manuscripts are published online shortly after acceptance, before technical editing, formatting and proof reading. Using this free service, authors can make their results available to the community, in citable form, before we publish the edited article. We will replace this *Accepted Manuscript* with the edited and formatted *Advance Article* as soon as it is available.

You can find more information about *Accepted Manuscripts* in the Information for Authors.

Please note that technical editing may introduce minor changes to the text and/or graphics, which may alter content. The journal's standard Terms & Conditions and the Ethical guidelines still apply. In no event shall the Royal Society of Chemistry be held responsible for any errors or omissions in this *Accepted Manuscript* or any consequences arising from the use of any information it contains.

ROYAL SOCIETY OF CHEMISTRY

www.rsc.org/njc

Multiplexing determination of lung cancer biomarkers using electrochemical and surface-enhanced Raman spectroscopic techniques

Wenbo Lu, Ying Wang, Xiaowei Cao, Li Li, Jian Dong, Weiping Qian*

State Key Laboratory of Bioelectronics, School of Biological Science and Medical Engineering, Southeast University, Nanjing 210096, China

**Corresponding author: Tel: (+86)25-83795719; Fax: (+86)25-83795719. E-mail: wqian@seu.edu.cn*

Abstract

A simple multiplexed electrochemical and surface-enhanced Raman spectroscopic (SERS) immunosensor is developed for simultaneous detection of carcinoembryonic antigen (CEA) and cytokeratin-19 (CK-19). We find a kind of Raman dye (Thionine and Nile blue A)-decorated resin microspheres by π-π stacking interaction, which show both strong SERS signals and electrochemical redox characteristic peaks. Aminosalicylic acid-based resin (AAR) microspheres are synthesized by a template-free method for the first time. The Au nanoparticles (AuNPs) coated AAR microspheres (AuNPs/AAR) are prepared by a convenient reduction approach. A sandwich structure contains Raman dye-labeled AuNPs/AAR with the first antibody, the second antibody immobilized on the electrode modified chitosan stabilized AuNPs, and target antigens. Thus, in the presence of the target antigens, the Raman dye-labeled AuNPs/AAR could be bonded to the modified electrode surface by antibody–antigen–antibody interactions. Compared with thionine, the Nile blue A has different Raman signals and electrochemical characteristic peaks. As a result, a simultaneous immunoassay for CEA and CK-19 based on multiple labels is fabricated by using electrochemical and SERS immunoassays. The prepared immunoassay for detection of CEA and CK-19 shows high sensitivity, selectivity, low detection limit and long term stability. The lowest detectable concentration is 0.01 ng/mL and 0.04 ng/mL for CEA and CK-19 at a signal to noise rate of 3, respectively. The proposed immunosensor can be applied to determine CEA and CK-19 in human blood serum with favorable results. In addition, the electrochemical and SERS immunosensor has potential application in diagnosis and treatment of lung cancer in the clinical research.

Keywords: Immunosensor; SERS; electrochemical; carcinoembryonic antigen; cytokeratin-19.

1. Introduction

Lung cancer is the leading cancer killer, and an estimated 13% of all deaths are expected to die from lung cancer each year [1]. Lung cancer is a kind of malignant tumor, which is characterized by uncontrolled cell growth in tissues of the lung. The uncontrolled cell will spread into nearby tissue or other parts of the human body through these metabolic processes [2]. A number of cancer patients are carcinomas which is derived from epithelial cells. The main types of lung cancer are classified as small-cell lung carcinoma and non-small-cell lung carcinoma [2]. Non-small-cell lung cancer holds on the most common cause of cancer-related death in the world. Scientists have made great progress in the identification of lung tumor-associated markers, especially in human tissue and serum [3-7]. The biomarkers are the important basis to detect lung cancer cells, including cytokeratin-19 (CK-19) and carcinoembryonic antigen (CEA) [8]. CK-19 is the most used marker for detection of lung tumor cells disseminated in lymph nodes, which is responsible for the structural cell integrity of epithelial cells [8]. CEA is a kind of membrane cellular adhesion molecules, which plays a important role in participating in cellular adhesion to endothelium [9]. The quantitative detection of protein biomarkers plays a key role in the clinical cancer screening, disease diagnosis, evaluating therapeutic interventions and monitoring of cancers [10]. The simultaneous measurement of multiple biomarkers can improve the diagnostic accuracy. Therefore, the development of a new preparation strategy for simultaneous determination of two or more biomarkers is highly desired in clinical diagnosis.

Raman spectroscopy is an available spectroscopic technique used to provide signals with important information in biomolecular systems [11]. Nonetheless, Raman spectra fails to be widely used for highly sensitive quantitative and qualitative analyses, due to its weaken signals. Surface-enhanced Raman scattering (SERS) has become a high sensitive analytical technique because it can tremendously enhance the Raman intensity of molecules adsorbed on rough surface of noble metals [12]. The surface enhancement factors of SERS signals range from 10^3 to 10^{14} [13]. SERS is usually applied to identifying protein and fabricating immunoassays. SERS-based immunoassay technique using functional nanomaterials have drawn widespread attention because it has been used as a potential candidate for multiplex detection [14]. Meanwhile, electrochemical sensors for immunoassays have attracted increasing attention due to the sensitive and convenient label-free advantage [15]. Electrochemical immunosensor for simultaneous detection of multiple biomarkers is mainly divided into two types, which is based on spatial resolution and multiple labels. The one type needs the multiple electrode to capture antibodies or antigens [16]. Nevertheless, this type is limited for applicaton due to its high consumption and multi-steps. As for the other type, multiple-labeled molecules and antibodies decorated on materials are selectively bonded to the surface of electrode by the single-step sandwich immunoreaction. The detection of simultaneous multianalytes can be obtained in a single electrochemical run with simple operation. The electrochemical immunosensors and SERS-based immunoassay technique are two powerful approaches for biomarkers determination. The electrochemical and

SERS-based immunoassays offer many advantages, such as low cost, simple operation, linear detection and high sensitivity [11-16]. However, the electrochemical and SERS-based immunoassays have their own shortcomings. For electrochemical immunoassay, the biomarkers are easy to fall off the substrate in the electrolyte solution; while the SERS-based immunoassay does not exist this problem. For SERS-based immunoassay, the detection area is limited when using a small spot of Raman laser; but the whole area of the substrate can be detected by the electrochemical immunoassay. For electrochemical immunoassay, the chemical properties of signaling molecules may change because of the redox reaction process; while the chemical properties usually do not change in SERS-based immunoassay. Therefore, to develop an effective and reliable strategy using the complementary advantages of the electrochemical and SERS technologies is highly desired.

Here, we demonstrate a kind of Raman dye (Thionine and Nile blue A)-decorated resin microsphere composites by π-π stacking interaction, which show both strong SERS signals and electrochemical redox characteristic peaks. Aminosalicylic acid-based resin (AAR) microspheres are synthesized by a surfactant-free and template-free method for the first time. The Au nanoparticles (AuNPs) coated AAR microspheres (AuNPs/AAR) prepared by a convenient reduction approach show good stability. A sandwich structure contains the Raman dye (Thionine and Nile blue A)-labeled AuNPs/AAR with the first antibody, the second antibody immobilized on the electrode modified chitosan stabilized AuNPs, and target antigens. Thus, in the presence of the target antigens, the Raman dye-labeled

AuNPs/AAR could be bonded to the modified electrode surface by antibody–antigen–antibody interactions. Compared with thionine, the Nile blue A has different Raman signals and electrochemical characteristic peaks. As a result, a simultaneous immunoassay for CEA and CK-19 based on multiple labels is fabricated by using electrochemical and SERS immunoassays. The prepared immunoassay for detection of CEA and CK-19 shows high sensitivity, low detection limit and long term stability. To the best of knowledge, it is the first time that the AuNPs/AAR have been used as a immunosensor for the detection of CEA and CK-19 by using electrochemical and SERS techniques. The proposed immunosensor can be applied to determine CEA and CK-19 in human blood serum with favorable results.

2. Materials and methods

2.1 Materials

4-Aminosalicylic acid (98 wt%), Bovine serum albumin (BSA), Vitamin C, 1-Ethyl-3-(3-dimethylaminopropyl)carbodiimide (EDC), N-Hydroxysuccinimide (NHS), Glycine, glucose, ammonium hydroxide (NH_3•H_2O) (28 wt% in water), formaldehyde (37 wt%), were purchased from Aladin Ltd. (Shanghai, China). Chloroauric acid solution ($HAuCl_4$•$4H_2O$) were purchased from Sinopharm Chemical Reagent Co., Ltd. (Shanghai, China). NaH_2PO_4, Na_2HPO_4, ethanol were purchased from Beijing Chemical Reagent (Beijing, China). Alpha fetoprotein (AFP) standard grade antigens, CEA standard grade antigens, CK-19 (Cyfra21-1) standard grade antigens, and anti-CEA antibodies, anti-CK-19 (anti-Cyfra21-1) antibodies were

purchased from Linc-Bio Science Co. (Shanghai, China). All chemicals were used as received without further purification. The water used throughout all experiments was purified through a Millipore system. Phosphate buffer saline (PBS) was prepared by mixing stock solutions of NaH_2PO_4 and Na_2HPO_4. Human blood samples were kindly provided by the Hospital of Southeast University. These human serum samples were prepared from human blood. The human serum was separated from the blood samples by centrifugation. Human serum samples were diluted to different concentrations with a PBS solution of pH 6.5, and each sample was analyzed for three times.

2.2 Instruments and characterization

Fourier Transform Infrared spectroscopy (FT-IR) measurements were made on a FT-IR Spectrometer TENSOR 27 (Bruker Optik GmbH, Ettlingen, Germany). Transmission electron microscopy (TEM) measurements were made on a HITACHI H-8100 EM (Hitachi, Tokyo, Japan) with an accelerating applied potential of 200 kV. The sample for TEM characterization was prepared by placing a drop of the dispersion on carbon-coated copper grid and dried at room temperature. Scanning electron microscopy (SEM) measurements were made on a XL30 ESEM FEG scanning electron microscope at an accelerating applied potential of 20 kV. The sample for SEM characterization was prepared by placing a drop of the dispersion on a bare Si substrate and air-dried at room temperature. Electrochemical measurements were performed with a CHI 660D electrochemical analyzer (CH Instruments, Inc., Shanghai). A conventional three electrode cell was used, including a GCE (geometric area = 0.07 cm^2) as the working electrode, a Ag/AgCl (3 M KCl) electrode as the

reference electrode, and platinum foil as the counter electrode. All potentials given in this work were referred to the Ag/AgCl electrode. All the experiments were carried out at ambient temperature. The Raman experiments were collected with a Renishaw Invia Reflex system equipped with Peltier-cooled charge-coupled device (CCD) detectors and a Leica microscope. Samples were excited with a He–Ne laser (785 nm) with a spot size of approximately 2 μm and power density of around 3×10^4 W cm^2.

2.3 Synthesis

2.3.1 Synthesis of AAR microspheres

In a typical synthesis, 0.0426 g of 4-Aminosalicylic acid (98 wt%) was added into 12 mL of ethanol and 5 mL of water, followed by adding 77 μL of ammonia aqueous solution (NH_4OH, 28 wt%) to form a homogeneous solution for 20 min at 35 ℃. After the addition of 62 μL of formaldehyde solution (37 wt%), the resulting mixed solution was stirred at 40 ℃ for 4.5 h and subsequently heated at 110 ℃ for 24 h in a Teflon-lined autoclave. The AAR microspheres were purified with distilled water and ethanol by centrifugation at a speed of 4000 rpm for 3 times, respectively. The resulting precipitates (AAR microspheres) were re-dispersed in 10 mL of water for characterization and further use.

2.3.2 Synthesis of AuNPs/ AAR microspheres

In a typical synthesis, 1 mL of the as-prepared AAR microspheres was dispersed in deionized water (9 mL) and 200 μL of 24.3 mM $HAuCl_4$ solution, and then the mixture solution was stirred for 30 min. Next, 100 μL of 0.15 M $NaBH_4$ aqueous solution were added into the previous solution under stirring for 30 min at room

temperature. The AuNPs decorated AAR microspheres (AuNPs/AAR microspheres) were purified with distilled water by centrifugation at a speed of 4000 rpm for 3 times. The resulting AuNPs/AAR microspheres were re-dispersed in 1 mL of water for characterization and further use.

2.3.3 Synthesis of CHIT-AuNPs composites

Chitosan-stabilized AuNPs (CHIT-AuNPs) were prepared via reduction of $HAuCl_4$ by $NaBH_4$. In brief, 100 μL of 24.3 mM $HAuCl_4$ aqueous solution was introduced into 10 mL of 0.5 % chitosan solution under stirring for 60 min. Then 100 μL of $NaBH_4$ (0.1 M) was added to the resulting mixture, and stirred for 60 min. As-formed CHIT-AuNPs dispersion was stored at 4 ^{o}C for further use.

2.3.4 Synthesis of immunocomposites

1 mL AuNP/AAR microspheres dispersion was added into 4 mL of 2 mg/mL thionine (THI) solution. After stirring for 60 min, the THI/AuNPs/AAR microspheres were formed. The as-prepared composites (THI/AuNPs/AAR) were collected by several centrifugation and washing with water. 1 mL AuNPs/AAR microspheres dispersion was added into 4 mL of 0.2 mM Nile blue A (NBA) solution. After stirring for 60 min, the NBA/AuNPs/AAR microspheres were prepared. The as-prepared composites (NBA/AuNPs/AAR) were collected by several centrifugation and washing.

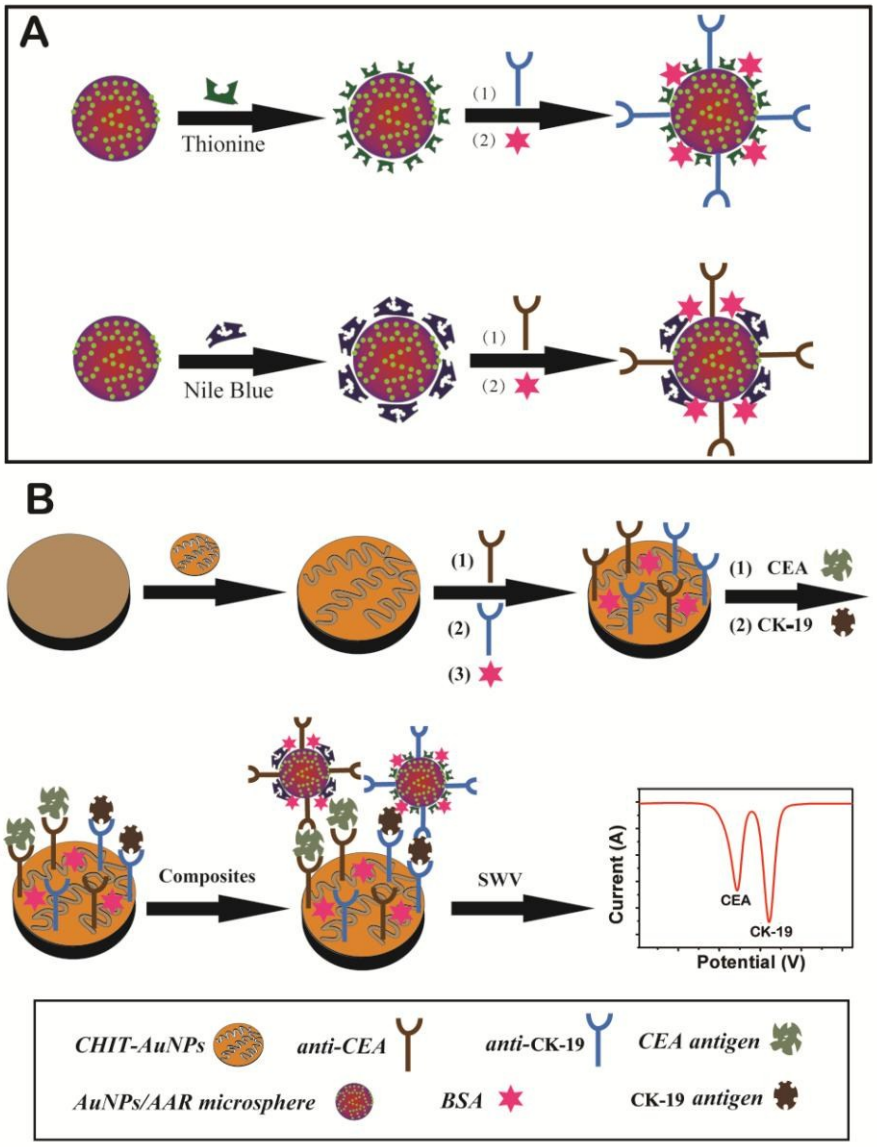

Scheme 1 (A) Schematic illustration of synthesis procedure of anti-CK-19/THI/AuNPs/AAR and anti-CEA/NBA/AuNPs/AAR composites. (B) The measurement protocol of the electrochemical immunosensor fabrication procedure.

Then, the prepared THI/AuNPs/AAR microspheres were dispersed in 2 mL PBS solution containing EDC and NHS, and reacted for 1 h. Then the composites were centrifuged at 4000 rpm for 8 min to remove excessive EDC and NHS, and the precipitation was dispersed in 1 mL PBS solution. Subsequently, 100 μg/mL of anti-CK-19 was added into the above mixture and gently mixed for 10 h. After

centrifugation, the obtained composites were reacted with 1 % (wt %) BSA solution for 2 h to block any possible remaining active sites to avoid any nonspecific absorption. After centrifuged, the resulting composites (anti-CK-19/**THI**/AuNPs/AAR) were re-dispersed in 1 mL of PBS solution for characterization and further use. The preparation process of anti-CEA/**NBA**/AuNPs/AAR composites were the same with anti-CK-19/**THI**/AuNPs/AAR composites. Scheme 1A schematic illustration of synthesis procedure of anti-CK-19/**THI**/AuNPs/AAR and anti-CEA/**NBA**/AuNPs/AAR composites.

2.4 Preparation of the immunosensor

Prior to the surface coating, the GCE was polished with 1.0 and 0.3 μm alumina powder, respectively, and rinsed with doubly distilled water, followed by sonication in ethanol solution and distilled water successively. Then, the electrode was allowed to dry in a stream of nitrogen. Firstly, 3 μL CHIT-AuNPs solution was dropped on the surface of pretreated GCE and left to dry at room temperature. Then the CHIT-AuNPs decorated GCE was immerged into the PBS solution containing EDC and NHS, in order to activate carboxyl of chitosan. After washing, 100 μg/mL of anti-CK-19 and anti-CEA were immediately dropped on the surface of the modified electrode and then incubated for 2 h to form the anti-CK-19/CHIT-AuNPs/GCE and anti-CEA/CHIT-AuNPs/GCE. Following that, this modified electrode was washed and incubated in 1 wt% BSA solution for 60 min to eliminate nonspecific binding. The immunosensor was first incubated with the PBS solutions or serum samples with various concentrations of CK-19 and CEA for 30 min at 37 ^{o}C. Then, it was incubated

with the mixture of anti-CK-19/**THI**/AuNPs/AAR and anti-CEA/**NBA**/AuNPs/AAR composites dispersion (the excessive composites use). After every step, the immunosensor were performed to record the electrochemical responses and SERS signals for simultaneous measurement of CK-19 and CEA in PBS solutions (pH 6.5). Scheme 1B displays the measurement protocol of the electrochemical immunosensor fabrication procedure.

2.5 Application in analysis of human serum samples

Human blood samples were kindly provided by the Hospital of Southeast University. The human serum samples were separated from the blood samples by centrifugation. Human serum samples were diluted to different concentrations with a PBS solution of pH 6.5. Three selected human serum samples (containing 10 ng/mL, 20 ng/mL and 30 ng/mL of CEA and CK19) are prepared by diluting CEA and CK19 standard sample using the human serum. The immunoassay for three selected samples is determined by the enzyme-linked immunosorbent assay (ELISA). Each human serum samples were tested for five times. The data of the human serum samples (monitoring the absorbance at 450 nm) were measured against a background control using a microplate reader (Thermo-scientific, Mullikan FC, USA).

3. Results and discussion

3.1 Characterization of AuNPs/AAR microspheres

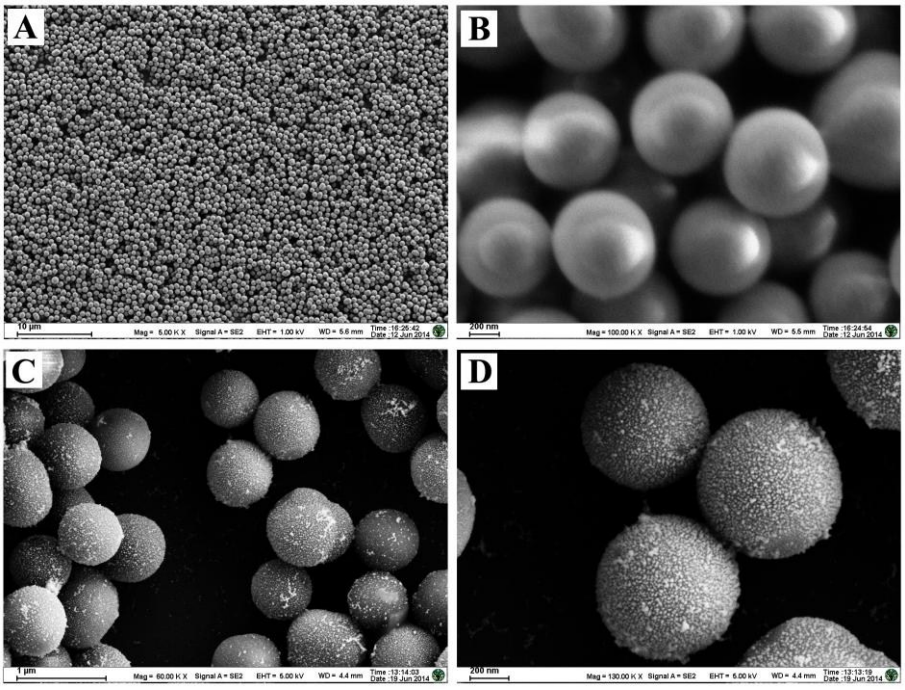

Figure 1 (A) Low and (B) high magnification SEM images of the AAR microspheres. (C) Low and (D) high magnification SEM images of the AuNPs/ARR microspheres.

Figure 1A shows the low magnification SEM image of the AAR microspheres, indicating that they consist of a large amount of colloidal spheres. The high magnification SEM image shown in Figure 1B further reveals that the AAR microspheres are about 400 nm in diameter. Figure S1 shows the chemical composition of the AAR microspheres is determined by the energy-dispersed spectrum (EDS). The peaks of C, N, an O elements are observed, indicating that they are formed from 4-aminosalicylic acid and ethanol (other peaks originated from the Si substrate). The preparation process of AAR microspheres is based on the polymerization reaction of 4-aminosalicylic acid and formaldehyde in the mixture solutions of water and ethanol. The AuNPs/AAR microspheres are prepared by a convenient reduction approach. Figure 1C shows the low magnification SEM images

of AuNPs/AAR microspheres, which consists of a large number of microspheres. A large amount of nanoparticles are adsorbed on the surface of AAR microspheres, as shown in Figure 1D. The chemical composition of the AuNPs/AAR microspheres is also determined by the corresponding EDS. The C, O and N elements are also observed in the EDS image of the AuNPs/AAR microspheres, as shown in Figure S2. The C, O, and N elements are derived from resin microspheres formed from 4-aminosalicylic acid. Compared with the EDS image of AAR microspheres (Figure S1), an additional peak of Au element is observed, suggesting that the nanoparticles are AuNPs. The AAR microspheres are provided with hydroxyl and epoxy functional groups. The functional groups have been used as anchors for adsorption of polar materials and inorganic nanoparticles. Au^{3+} ion can be adsorbed onto the carboxylic group of AAR microspheres through electrostatic attraction. The reduction of these Au^{3+} ions by sodium borohydride allows these AuNPs to attach onto the surface of AAR microspheres. All the above observations indicate that the AuNPs/AAR microspheres are formed successfully.

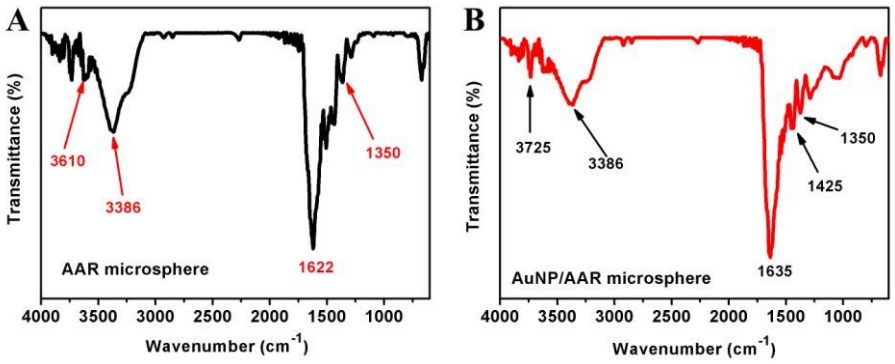

Figure 2 FT-IR spectra of the AAR microspheres (A) and AuNPs/AAR microspheres (B).

Figure 2A shows FT-IR results of the AAR microspheres. The appearance of a

weak band at 3610 cm^{-1} is attributed to the presence of -OH groups on the surface of the as-prepared AAR microspheres [17]. The broad and intense peak observed at 3386 cm^{-1} can be attributed to the -OH groups [18]. The peak observed at 1350 cm^{-1} can be attributed to the C-N stretching or N-H in-plane bending vibration [19], which indicates the existence of the amino group. The peak at 1622 cm^{-1} is attributed to the AAR microspheres stretch of the carboxylic (-COOH) group [20].It is observed that the bonds of the -OH groups, the carboxylic (-COOH) group, and the amino groups are presented in the AAR microspheres, indicating that AuNPs can be easily adsorbed on the exterior of AAR microspheres. FT-IR spectra of AuNPs/AAR microspheres are also measured in Figure 2B. The band at 1635 cm^{-1} is assigned to the C=O stretching [21], indicating the existence of the carboxylic (-COOH) group. A sharp band at 3,725 cm^{-1} is attributed to the -OH absorption [22]. The peak of the -OH absorption bands are also observed at 3386 cm^{-1} [18], as shown in Figure 2B. After the contact with AuNPs, the bonds of the -OH groups and the carboxylic (-COOH) group is also observed in the FT-IR spectrum of the AuNPs/AAR microspheres. The functional group of the AuNPs/AAR microspheres still remain its inherent properties, which can provide a favorable microenvironment for immobilization of antibodies. Figure S3 shows the FT-IR spectrum of anti-CK-19/anti-CEA/AuNP/AAR microspheres. The peak at 1649 cm^{-1} is assigned to the C=O symmetric stretching band of C=O group [23]. The peak at 1551 cm^{-1} is characteristic asymmetric stretching modes in –CONH- of antibody [23], indicating that the anti-CK-19 and anti-CEA are successfully modified on the AuNP/AAR microspheres.

3.2 Electrochemical characterization of the immunosensor

The immunosensor is fabricated by the sandwich-type immunocomposites between the CHIT-AuNPs/GCE and AuNPs/AAR microspheres for CEA and CK-19. When both CEA and CK-19 antigens are present in buffer solution, the CHIT-AuNPs/GCE and AuNPs/AAR microspheres will form a sandwich composites by antibody–antigen–antibody interactions; however, they will not form a sandwich composites in the absence of antigens. The fabrication process of the electrochemical immunosensor and measurement procedure is described in Scheme 1B. The Electrochemical impedance spectroscopy (EIS) measurements are performed in 5 mM $[Fe(CN)_6]^{-3/-4}$ solution with the purpose of monitoring the fabrication process of the immunosensor. In the Nyquist diagram, the linear portion at the low frequencies and the semicircle portion at the high frequencies correspond to the diffusion-limited process and the electron transfer-limited process, respectively. The electron transfer resistance (Ret) can be estimated from the diameter of a semicircle in an impedance spectrum.

Figure 3 shows the complex impedance plots of different layer modified electrode in 5.0 mM $[Fe(CN)_6]^{4-/3-}$ solution. It is observed that the bare GCE exhibits a small semicircle at high frequencies with a diameter of 216 ohm and a linear part at low frequencies (line a of Figure 3), which is characteristic of a diffusional limiting step of the electrochemical process on a bare GCE. After deposition of CHIT-AuNPs composites (line b of Figure 3), the Ret of 174 ohm is much smaller than that of the bare GCE, indicating that the CHIT-AuNPs composites can promote the electron

transfer. When the anti-CEA and anti-CK-19 are adsorbed to the CHIT-AuNPs/GCE (anti-CK-19/anti-CEA/CHIT-AuNPs/GCE) (line c of Figure 3), the value of Ret increased to 252 ohm. The result is ascribed to the nonconductive properties of anti-CEA and anti-CK-19, which insulate the conductive support and block the electron transfer. Similarly, after the capture of BSA, CEA and CK-19, the values of Ret increase to 281 ohm and 383 ohm, respectively. It is suggested that the formation of hydrophobic immunocomplex layer hinders the electron transfer. All these observations demonstrate that the CHIT-AuNPs composites, anti-CEA, anti-CK-19, BSA, CEA and CK-19 have been successively assembled on to the surface of GCE.

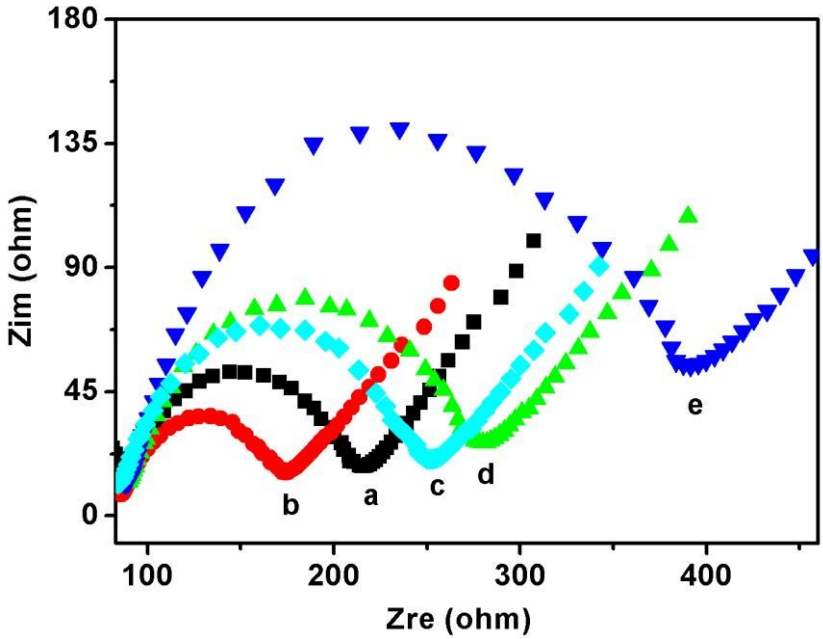

Figure 3 EIS performed in $[Fe(CN)_6]^{4-/3-}$-PBS solution containing 0.1 M KCl: (a) bare GCE; (b) CHIT-AuNPs/GCE; (c) anti-CK-19/anti-CEA/CHIT-AuNPs/GCE; (d) anti-CK-19/anti-CEA/CHIT-AuNPs/GCE blocked with 1 % BSA; and (e) modified GCE electrode after incubation with 10 ng/mL of CEA and CK-19.

3.3 Selection of signal molecules

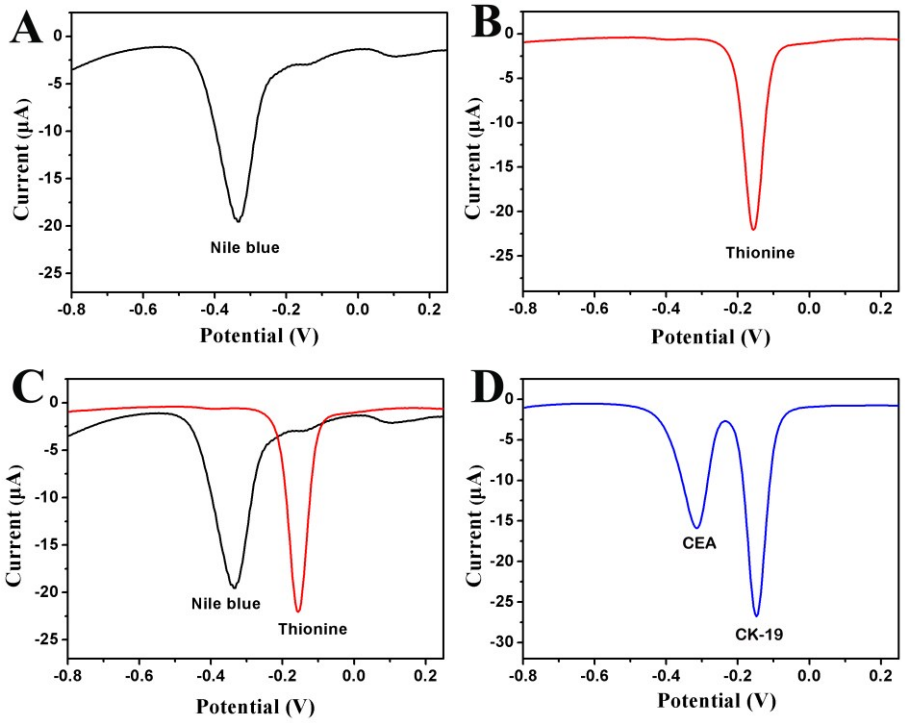

Figure 4 Square wave voltammograms (SWVs) of (A) NBA/AuNPs/AAR/GCE, (B) THI/AuNPs/AAR/GCE, and (D) the immunosensor in 0.1 M PBS at pH: 6.5 (scan rate: 50 mV/s). (C) The composite curves between curve A and curve B.

To testify the sensing application of the AuNPs/AAR microspheres, the feasibility of the immunosensor is investigated in this study. The redox molecules (THI and NBA) are absorbed on the surface of these microspheres. Figure 4A shows the SWV (Square wave voltammogram) responses of the NBA/AuNPs/AAR microspheres decorated GCE (NBA/AuNPs/AAR/GCE) in PBS solution. A reduction peak can be obviously seen in Figure 4A. The peak at -0.33 V vs. Ag/AgCl should consider as the electrode toward the reduction of NBA. Figure 4B shows the SWV responses of the THI/AuNPs/AAR microspheres decorated GCE (THI/AuNPs/AAR/GCE) in PBS solution. The peak at -0.15 V is observed, which is assigned to the reduction of THI in the THI/AuNPs/AAR microspheres. The SWVs of

NBA/AuNPs/AAR/GCE and THI/AuNPs/AAR/GCE are put into one figure in Figure 4C. A clear distinction between the positions of two peaks is seen in Figure 4C. The SWV responses of the prepared immunosensor in PBS solution are also tested, two reduction peaks are observed in Figure 4D. As a result, the redox molecules (THI and NBA) can be used as signal reporters to detect two lung cancer biomarkers.

3.4 Optimization of detection conditions

The electrochemical performance of the immunosensor would be influenced by many factors. The pH of the solution has a great effect on the electrochemical behavior of the immunosensor, because the activity of the immobilized protein may be influenced by the acidity of the solution [24]. In order to optimize the pH, a series of PBS buffer with the pH from 4.0 to 8.0 are prepared and the immunosensors are tested by SWV. When pH increases from pH 4.0 to 6.5, the reduction peak current will get higher and reach the maximum value at pH 6.5, and then decreases to pH 8.0, as shown in Figure S4A. Figure S4C shows that the current response of the THI/AuNPs/AAR/GCE increases from pH 4.0, reaches the maximum value at pH 6.5, and then decreases to pH 8.0. As a result, pH 6.5 is chosen as the optimal pH of the detection solution to obtain a high sensitivity. Incubation time is another important parameter in the construction of the immunosensor. The effect of incubation time is investigated in the time range of 5–40 min with 10 ng/mL of CEA. Figure S4B shows that the current response rapidly decreases within the first 30 min and then tends to level off due to the saturated formation of antigen-antibody complex. For the incubation time of CK-19, the similar results are observed in Figure S4D. Therefore,

the optimal incubation time is set at 30 min.

3.5 Analytical performance of the electrochemical immunosensor

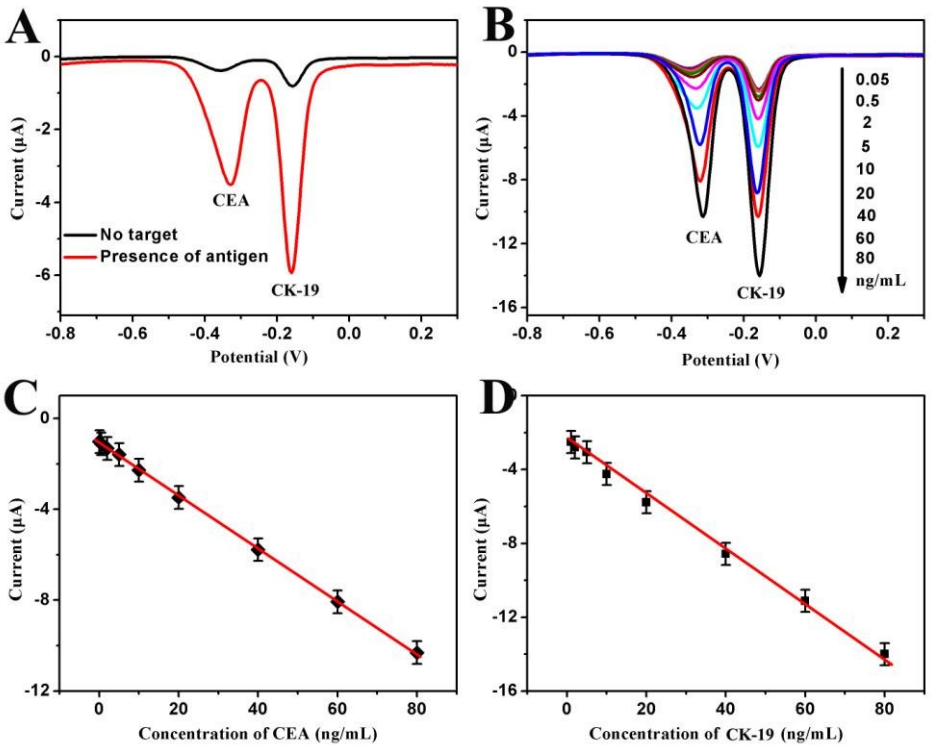

Figure 5 (A) SWV responses of the immunosensor for blank control (blcak line) and a mixture of 10 ng/mL CEA and 10 ng/mL CK-19 solutions in 0.1 M PBS solution. (B) SWV responses of the immunosensor after incubation with various concentrations of CEA and CK-19. The calibration plots of the multiplex immunoassay toward CEA (C) and CK-19 (D) in 0.1 M PBS (pH: 6.5) solution.

In order to investigate the cross-reactivity between antigens and the composites (anti-CK-19/**THI**/AuNPs/AAR and anti-CEA/**NBA**/AuNPs/AAR), the two control tests are carried out. The immunosensor incubated with PBS solution in absence of CK-19 and CEA, is tested using the anti-CK-19/**THI**/AuNPs/AAR and anti-CEA/**NBA**/AuNP/AAR composites as electrochemical signal tags. It is obviously

seen that the current peaks of SWV are quite weak, as shown in Figure 5A (black line). In presence of CK-19 and CEA, the corresponding peak current was extremely obvious, as shown in Figure 5A (red line). All above observations indicate that the cross-reactivity could be nearly ignored.

The performance of the electrochemical immunoassay is evaluated using CEA and CK-19. Figure 5B shows the SWV peak currents of the immunosensor increased with the concentrations of CEA and CK-19 increased. Typically, the redox composites (anti-CK-19/**THI**/AuNPs/AAR and anti-CEA/**NBA**/AuNPs/AAR) were attached to the electrode surface through immunoreaction with CK-19 and CEA which were immobilized on the immunosensor previously. The redox composites are used as electrochemical signals to monitor the concentrations of CEA and CK-19. Therefore, the SWV peak currents increased proportionally with the increasing concentration of CEA and CK-19, which can be utilized as a quantitative measurement of CK-19 and CEA concentration. The calibration curves exhibit a good linear relationship between the reduction peak currents and the concentrations of CEA and CK-19 in the range from 0.05 to 80 ng/mL, as shown in Figure 5C and Figure 5D. The correlation coefficient is 0.997 for CEA and 0.993 for CK-19. The lowest detectable concentration is 0.01 ng/mL and 0.04 ng/mL for CEA and CK-19 at a signal to noise rate of 3, respectively. The analytical performance of the proposed immunosensor has been compared with the CEA and CK19 immunosensors reported previously. Table 1 compares the sensing performance of different immunosensors for CEA and CK-19, showing our proposed immunosensor exhibits a lower detection limit than the results

of previously reported sensing systems.

Table 1 Comparison of different immunosensors for detection of CEA and CK-19.

Immunosensors	Detection limit (ng mL^{-1})		References
	CEA	CK-19	
Europium and samarium chelates	0.85	0.77	25
Radioimmunometric assay	3	15	26
Solid-phase immunoradiometric assay	6.5	2.0	27
AuNP/AAR microspheres	0.01	0.04	This work

3.6 Analytical performance of the SERS-based immunosensor

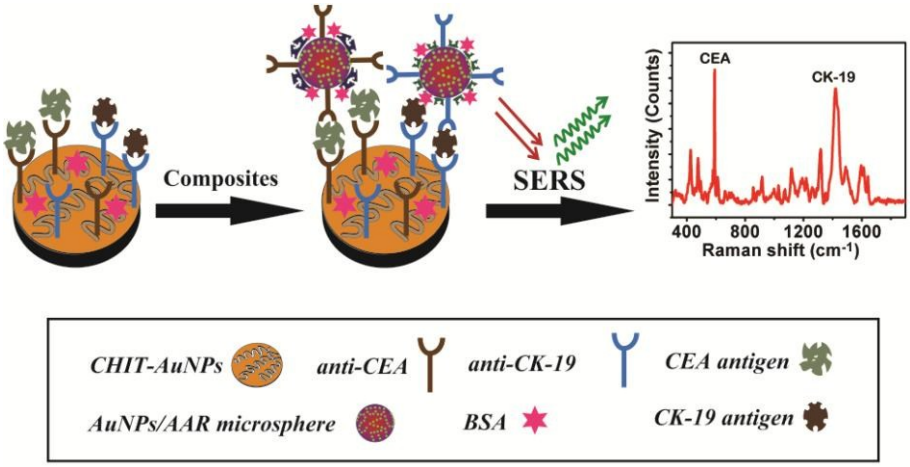

Scheme 2 Schematic illustration of the preparation of SERS-based immunoassay.

SERS-based immunoassay has been deeply investigated between qualitative and quantitative, which is a promising technique for highly sensitive detection of lung cancer biomarkers [5]. When a mixture of CEA and CK-19 are present in sample solution, Raman dye (THI and NBA)-decorated resin microsphere composites (anti-CK-19/**THI**/AuNPs/AAR and anti-CEA/**NBA**/AuNPs/AAR) can be bonded to the modified electrode surface by antibody–antigen–antibody interactions. After trapping the immunocompposites, the SERS signal was measured by Renishaw

Raman spectrometers. However, they do not form a immunocompposites in the absence of antigen. A clear distinction between the positions of two peaks of THI and NBA can be observed. Therefore, the Raman dye molecules (THI and NBA) can be used as Raman signal reporters to detect two lung cancer biomarkers.

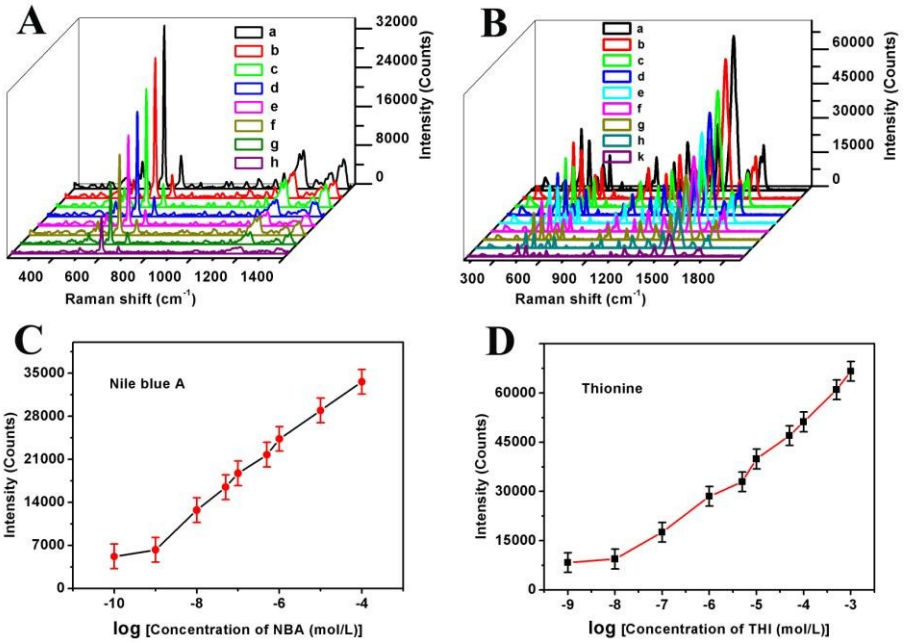

Figure 6 (A) Representative 785 nm excited SERS spectra with different concentrations of NBA : (a) 1×10^{-4} M, (b) 1×10^{-5} M, (c) 1×10^{-6} M, (d) 5×10^{-7} M, (e) 1×10^{-7} M, (f) 5×10^{-8} M, (g) 1×10^{-8} M, (h) 1×10^{-9} M on AuNPs/AAR microspheres. (C) A logarithmic plot of NBA concentration and the intensity of SERS signal for the bands at 592 cm^{-1}. (B) Representative 785 nm excited SERS spectra with different concentrations of THI : (a) 1×10^{-3} M, (b) 5×10^{-4} M, (c) 1×10^{-4} M, (d) 5×10^{-5} M, (e) 1×10^{-5} M, (f) 5×10^{-6} M, (g) 1×10^{-6} M, (h) 1×10^{-7} M, (k) 1×10^{-8} M on AuNPs/AAR microspheres. (D) A logarithmic plot of THI concentration and the intensity of SERS signal for the bands at 1390 cm^{-1}.

The metallic nanomaterials exhibit high SERS activity, due to an increased field at the metallic nanoparticle surface which is a consequence of the interaction of the incoming laser radiation with electrons in the metal surface or collective oscillations

of the metal electrons [28]. In order to study the SERS activity of the AuNPs/AAR microspheres, the SERS activities of the AuNPs/AAR microsphere decorated substrates are tested by using two organic molecules (THI and NBA). NBA is often employed in SERS studies because of its unique Raman characteristic peaks. Figure 6A shows the obtained SERS spectra when different concentrations (1×10^{-9} M up to 1×10^{-4} M) of NBA solutions were tested. As shown in Figure 6A, the typical SERS spectra of NBA are characterized by the prominent strong bands at 592, 625, and 1167 cm^{-1}. The peak of NBA at 592 cm^{-1} is chosen as reference peak in our study. The SERS signals increased proportionally with the increasing concentration of NBA, which can be used as a quantitative measurement of NBA concentration. As shown in Figure 6C, the calibration plots show a linear relationship between the SERS signals and the logarithm values of the concentrations of NBA [(The dot (1×10^{-10} M) is removed, due to its SERS value is very close to another dot (1×10^{-9} M)]. It is obviously seen that there is a linear relationship between the SERS signals and the concentration of NBA over the range of 1×10^{-8} M up to 1×10^{-4} M with a correlation coefficient of 0.992, as shown in Figure 6C. Figure 6B shows the SERS spectra obtained when the substrate was immersed in solutions containing different concentrations of THI, following the same procedure from low to high concentration as that in the NBA measurements. The peak of the THI molecule at 1390 cm^{-1} is chosen as reference peak in our study [29]. The dot (1×10^{-9} M) is removed, due to its SERS value is very close to another dot (1×10^{-8} M), as shown in Figure 6D. It is obviously seen that there is a linear relationship between the SERS signals and the

concentration of THI over the range of 1×10^{-8} M up to 5×10^{-3} M with a correlation coefficient of 0.99, as shown in Figure 6D. As a result, our prepared AuNP/AAR microspheres show high SERS enhancing activity and can be used as SERS signals to detect two lung cancer biomarkers.

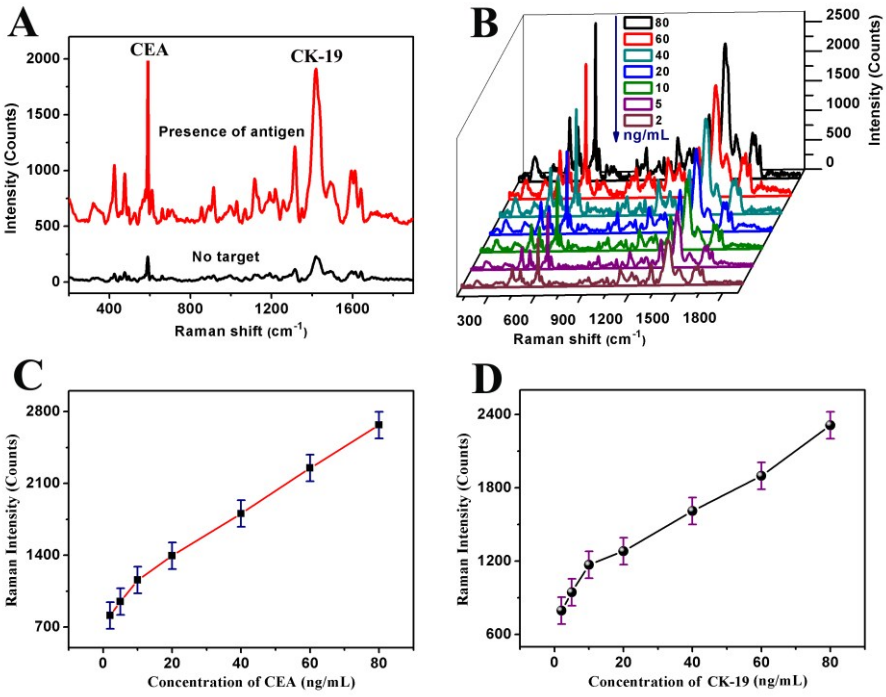

Figure 7 (A) Representative 785 nm excited SERS spectra of the immunosensors for blank control (blcak line) and a mixture of 20 ng/mL CEA and 20 ng/mL CK-19 solutions in 0.1 M PBS solution. (B) SERS spectra of the immunosensor after incubation with various concentrations of CEA and CK-19. The calibration plots of the multiplex immunoassay toward CEA (C) and CK-19 (D) in 0.1 M PBS (pH: 6.5) solution.

In SERS-based immunoassay, to investigate the cross-reactivity between antigens and the composites (anti-CK-19/**THI**/AuNPs/AAR and anti-CEA/**NBA**/AuNPs/AAR), two control tests are also carried out in our study. The SERS-based immunosensor incubated with PBS solution in absence of CK-19 and CEA, is tested using the anti-CK-19/**THI**/AuNPs/AAR and

anti-CEA/**NBA**/AuNPs/AAR composites as SERS signal tags. It is clearly seen that the SERS characteristic peaks are quite weak, as shown in Figure 7A (black line). In presence of CK-19 and CEA, the corresponding peak was extremely obvious, as shown in Figure 7A (red line). This indicates that the cross-reactivity could be almost ignored.

The performance of the SERS-based immunoassay is also evaluated with CEA and CK-19. Figure 7B shows the SERS peaks of the immunosensor increased with the increment concentrations of CEA and CK-19. Typically, the Raman dye-labelled composites (anti-CK-19/**THI**/AuNPs/AAR and anti-CEA/**NBA**/AuNPs/AAR) were attached to the substrates through immunoreaction with CK-19 and CEA which were immobilized on the immunosensor previously. The SERS intensity of the Raman dye-labelled composites are used as the signal tags to monitor the CEA and CK-19 concentrations. It is obviously seen that the SERS characteristic signals increased proportionally with the increasing concentration of CEA and CK-19. The calibration curves exhibit a linear relationship between the SERS peaks and the concentrations of CEA and CK-19 in the range from 2 to 80 ng/mL, as shown in Figure 7C and Figure 7D. The correlation coefficient is 0.992 for CEA and 0.975 for CK-19. The lowest detectable concentration is 0.62 ng/mL and 1.01 ng/mL for CEA and CK-19 at a signal to noise rate of 3, respectively. The analytical performance of the proposed SERS-based immunosensor has been compared with the above electrochemical immunosensor. It is found that performance of the electrochemical immunosensor is better that that of SERS-based immunosensor. As a result, the proposed

electrochemical immunosensor will applied to determine CEA and CK-19 in human blood serum compared with ELISA methods.

3.7 Application in analysis of serum samples

Analyte	CEA			CK-19		
Sample Number	Prepared sensor [ng/mL]	ELISA [ng/mL]	Relative error [%]	Prepared sensor [ng/mL]	ELISA [ng/mL]	Relative error [%]
1	30.8	30.1	2.32	29.1	30.2	-3.64
2	21.6	20.4	5.88	20.6	20.2	1.98
3	9.7	10.2	-3.96	9.6	10.4	-7.69

Figure 8 Assay results of clinical serum samples using the proposed immunosensor and the ELISA methods.

The feasibility of the prepared immunosensor for possibly clinical application is investigated by analyzing human serum samples from students of Southeast University Hospital. The immunoassay for human serum samples is investigated by analyzing three samples in comparison with ELISA technique. Each human serum sample is analyzed for ten times. Figure 8 shows the results and the relative errors between the two methods ranged from −3.96 % to 5.88 % for CEA and from −7.69 % to 1.98 % for CK-19. It is demonstrated that there is no signification difference between the results given by the two methods. As a result, the prepared immunosensor could be reasonably applied in the clinical determination of lung cancer biomarkers (CEA and CK-19).

3.8 Selectivity and stability of the immunosensor

The selectivity of the proposed immunosensor plays an important role in

analyzing biological samples without separation. Glucose, AFP, BSA, and glycine are used for the interferences study in CEA and CK-19 detection. Under the optimal conditions, the 10 ng/mL of CEA and CK-19 solution containing 50 ng/mL of interfering substances are measured by the immunosensor, as shown in Figure S5. Figure S4 shows that the changes of the reduction peak current response due to the interfering substances are less than 4.6 % for CEA and 2.1 % for CK-19 of that without interferences. All these observations indicate that the prepared immunosensor exhibits an acceptable selectivity for the detection of CEA and CK-19.

The stability of the immunosensors is evaluated over a period of seven days of storage (at 4 ^{o}C). After two days and seven days, the reduction peak current of the immunosensor decreases to approximately 93 % and 85 % of its initial value, respectively. Regeneration plays a key role in their application and development of immunosensors. After the immunosensor is used to detect CEA and CK-19, the immunosensor is treated with 1 M urea solution for 5 min to break the antibody–antigen linkage. When the immunosensor is repeated five times of consecutive measurements of one sample after the immunosensor is regenerated. The RSD of 7.9 % obtained at the 10 ng/mL of CEA and CK-19 solution. The results indicate that the immunosensor can be regenerated and used again. Based on the above mentioned observations, our proposed immunosensor could be applicably applied for the determination of CEA and CK-19 in the clinical diagnosis.

4. Conclusions

In summary, we report a kind of Raman dye-decorated Au nanoparticles/resin microspheres by π-π stacking interaction, which show both strong surface-enhanced Raman spectroscopic signals and electrochemical redox characteristic peaks. To take advantage of surface-enhanced Raman spectroscopic and electrochemical merit of the composites, an electrochemical and surface-enhanced Raman spectroscopic immunosensor is developed for simultaneous detection of carcinoembryonic antigen and cytokeratin-19. The prepared immunoassay for detection of carcinoembryonic antigen and cytokeratin-19 shows high sensitivity, selectivity, long term stability and reliability, due to the complementary advantages of the electrochemical and SERS technologies. This reliable and effective strategy for carcinoembryonic antigen and cytokeratin-19 determination has potential for application in diagnosis and treatment of lung cancer by using the two complementary technologies.

Acknowledgements

We gratefully acknowledge supports from the Chinese 973 Project (Grant: 2012CB933302), the National Natural Science Foundation of China (Grant: 21175022), the Ministry of Science & Technology of China (Grant: 2012AA022703), the Scientific Research Foundation of Graduate School of Southeast University (No.YBJJ1410), the Fundamental Research Funds for the Central Universities (No. 2242014Y10054) and Graduate Students' Scientific Research Innovation Project of Jiangsu Province Ordinary University (No.CXZZ13_0124).

References

[1] S.K. Arya, S. Bhansali, *Chem. Rev.,* 2011, **111**, 6783-6809.

[2] A. Alama, A. Truini, S. Coco, C. Genova, F. Grossi, *Drug Discovery Today,* 2014, **19**, 1671-1676.

[3] A. Wang, W. Ruan, W. Song, L. Chen, B. Zhao, Y.M. Jung, X. Wang, *J. Raman Spectroc.*, 2013, **44,** 1649-1653.

[4] V. Kulasingam, E.P. Diamandis, *Nat. Clin. Pract. Oncol.*, 2008, **5**, 588-599.

[5] H. Chon, S. Lee, S-Y. Yoon, S-I. Chang, D.W. Lim, J. Choo, *Chem. Commun.*, 2011, **47**, 12515-12517.

[6] H. Wang, Y. He, Y. Chai, R. Yuan, *Nanoscale,* 2014, **6**, 10316-10322.

[7] T. Xu, J. Ma, Z. Ma, *New J. Chem.,* 2015, **39**, 1006-1012.

[8] A. He, T.C. Liu, Z.N. Dong, Z.Q. Ren, J.Y. Hou, M. Li, Y.S. Wu, *J. Clin. Lab. Anal.*, 2013, **27**, 277-283.

[9] N. Liu, Z. Liu, H. Han, Z. Ma, *J. Mater. Chem. B,* 2014, **2**, 3292-3298.

[10] T. Xu, X. Jia, X. Chen, Z. Ma, *Biosens. Bioelectron.*, 2014, **56**, 174-179.

[11] D. Pappas, B.W. Smith, J.D. Winefordner, *Talanta,* 2000, **51**, 131-144.

[12] Z. Wang, S. Zong, H. Chen, H. Wu, Y. Cui, *Talanta,* 2011, **86**, 170-177.

[13] E. Tan, P. Yin, T. You, H. Wang, L. Guo, *ACS Appl. Mater. Interfaces,* 2012, **4**, 3432-3427.

[14] M.H. Shin, W. Hong, Y. Sa, L. Chen, Y.J. Jung, X. Wang, B. Zhao, Y.M. Jung, *Vibrat. Spectroscopy,* 2014, **72**, 44-49.

[15] X. Jia, X. Chen, J. Han, J. Ma, Z. Ma, *Biosens. Bioelectron.*, 2014, **53**, 65-70.

[16] F. Kong, B. Xu, Y. Du, J. Xu, H. Chen, *Chem. Commun.*, 2013, **49,** 1052–1054.

[17] M.V. Kandziolka, M.K. Kidder, L. Gill, Z. Wu, *Phys. Chem. Chem. Phys.*, 2014, **16**, 24188-24193.

[18] W. Sun, S. Shi, T. Yao, *Anal. Methods*, 2011, **3**, 2472-2474.

[19] S. Ling, Z. Qi, Z. Shao, X. Chen, *J. Mater. Chem. B,* 2015, **3**, 834-839.

[20] N. Sareen, S. Singh, S. Bhattacharya, *Dalton. Trans.*, 2014, **43**, 4635-4638.

[21] W. Niu, S. Wu, S. Zhang, *J. Mater. Chem.*, 2010, **20**, 9113-9117.

[22] Z. Lodziana, N.Y. Topsoe, J.K. Norskov, *Nat. Mater.*, 2014, **3**, 289-293.

[23] M. Li, S.K. Cushing, J. Zhang, S. Suri, R. Evans, W.P. Petros, L.F. Gibson, D. Ma, Y. Liu, N. Wu, *ACS Nano*, 2013, **7**, 4967-4976.

[24] E. Katz, I. Willner, *Angew. Chem. Int. Ed.*, 2005, **30**, 4869-4872.

[25] G. Lin, H. Zhao, T. Liu, J. Hou, Z. Ren, W. Huang, W. Dong, Y. Wu, *RSC Adv.*, 2014, **4**, 55229-55236.

[26] R.-S. Lai, C.-C. Chen, P.-C. Lee, J.-Y. Lu, *Jpn. J. Clin. Oncol.*, 1999, **29**, 421-424.

[27] B. Nakata, T. Takashima, Y. Ogawa, T. Ishikawa, K. Hirakawa, *British J. Cancer,* 2004, **91**, 873-878.

[28] E. Esenturk, A. Walker, *J. Raman Spectrosc.*, 2009, **40**, 86-91.

[29] H.R. Virdee, R.E. Hester, *Laser Chem.*, **1988**, *9*, 401-416.